Principal Component Image Analysis of MODIS for Volcanic Ash. Part I: Most Important Bands and Implications for Future GOES Imagers

DONALD W. HILLGER

NOAA/NESDIS/ORA/RAMMT, CIRA–Colorado State University, Fort Collins, Colorado

JAMES D. CLARK

NOAA/NESDIS/OSDPD/SSD Satellite Analysis Branch, Camp Springs, Maryland

(Manuscript received 9 August 2001, in final form 21 April 2002)

ABSTRACT

In Part I of this paper, the infrared bands of the Moderate Resolution Imaging Spectroradiometer (MODIS) are analyzed for volcanic ash signals using principal component image analysis. Target volcanoes included Popocatepetl volcano near Mexico City and Cleveland volcano in the Aleutian Islands. The analyses were performed to determine the MODIS bands that contribute the most to detecting volcanic ash. Even though the explained variance and signal-to-noise ratio of most of these new images are generally small, several of them provide views of volcanic ash with good contrast to the image background and other image features. Both day and night examples indicate that volcanic ash can be readily detected by combinations of MODIS bands to determine not only the ash extent but also qualitative variations in the concentration and height of the ash. The 36 bands on MODIS give much more flexibility for ash detection than the 4 bands on the current Geostationary Operational Environmental Satellite (GOES) Imager. In particular, MODIS bands 28–32, in the water vapor and longwave infrared portions of the spectrum, contributed most frequently to the detection of airborne volcanic ash. These include bands 28–30 in the 7.3–9.7-μm portion of the spectrum known for volcanic signals. Several of the MODIS bands that proved useful are bands projected for inclusion in the next major upgrade to the GOES Imager (scheduled for 2012). However, band 30 (9.7 μm) is neither available on the current GOES series nor planned for future GOES Imagers. In Part II of this paper, MODIS data for the same volcanic cases examined in Part I are used for specific simulations of current and near-term GOES imagery. The purpose of the simulations is to assess the impact of changes that will occur in the spectral bands of the GOES-M Imager (launched in 2001 and renamed *GOES-12*) when it becomes operational.

1. Introduction

The detection of volcanic ash clouds is of great importance for aviation meteorology. Volcanic ash represents an extreme hazard for aircraft. Several active volcanoes expel ash along major air traffic routes as well as in areas where normal meteorological reports are not as frequent as over the United States. Therefore satellite imagery is vital to volcanic ash detection. This paper will investigate the use of satellite imagery from new instrumentation and give recommendations for future satellite imagery needed for operational detection of volcanic ash.

Most current volcanic ash detection techniques rely heavily on split-window differencing of the thermal longwave infrared bands (centered at 11 and 12 μm) on current operational satellites (Prata 1989). However, this technique is not uniformly effective in properly classifying volcanic ash pixels in the satellite scene, often falsely interpreting meteorological cloud as volcanic ash cloud and vice versa (Simpson et al. 2000; Prata et al. 2001). One of the recommendations of the Simpson et al. study is that new research-grade satellite remote sensing instruments offering multispectral observations in the thermal infrared be used to better characterize eruptive events, and that the information be used to design improved volcanic ash cloud detection sensors. This will lead eventually to wider operational exploitation of these powerful and increasingly accessible technologies (Oppenheimer 1998).

One of the new satellite sensors currently available for research is the Moderate Resolution Imaging Spectroradiometer (MODIS; see MODIS Web site at: http://modis.gsfc.nasa.gov) MODIS imagery offers a multispectral advantage over Geostationary Operational Environmental Satellite (GOES) imagery for viewing volcanic ash and other atmospheric and surface features. The advantage is due to the larger number of spectral

Corresponding author address: Dr. Donald W. Hillger, NOAA/NESDIS/RAMMT, CIRA–Colorado State University, Fort Collins, CO 80523-1375.
E-mail: hillger@cira.colostate.edu

bands available on MODIS [36 bands: 19 bands in the visible and near-infrared (reflective), and 17 bands in the longer-wavelength infrared (thermal) portion of the earth's spectrum]. In comparison the GOES Imager has only five bands. In addition, some of the MODIS bands are in portions of the spectrum not sensed by GOES. However, this spectral advantage is offset by the lack of sufficient temporal resolution and continuity to follow rapidly changing phenomena as is customary from geostationary orbit. The MODIS instrument is currently on board the polar-orbiting Earth Observation Satellite (EOS) *Terra,* launched in December 1999. MODIS data are available for a minimum of two views of most earth locations during any 24-h period. MODIS will also be available from the recently launched EOS *Aqua,* which will lead to better temporal resolution and coverage.

All of the thermal infrared bands of MODIS are available at 1-km spatial resolution (at nadir). This is a horizontal resolution advantage over 4-km GOES infrared data, but that resolution advantage is not the focus of this study. MODIS data were either used at full resolution or reduced to 2-km resolution by sampling every other line and element. This choice of resolution was made to give the east–west or north–south spatial coverage necessary to see the full extent of the volcanic ash cloud in a given image size for the cases used in this study.

In section 2, the technique for detection of volcanic ash in satellite imagery will be discussed. Section 3 will cover both daytime and nighttime volcanic cases. Additional day and night cases will be analyzed in section 4. Section 5 will discuss the implications for future operational satellite image products for volcanic ash detection, leading to a summary and the conclusions in section 6.

2. Principal component imagery

In their study of volcanic clouds, Dean et al. (1994) found that satellite images analyzed using principal component techniques clearly distinguished the ash from its surroundings. Their preferred analysis technique utilized three-color composites of principal component and spectral band images to show the extent of the ash as well as its opaque and transparent properties. While typically applied to remote sensing of earth resources, principal component analysis (PCA) has been applied to GOES Imager and Sounder data to create principal component images (PCIs) for the detection of atmospheric and surface features in multiband imagery (Hillger 1996a,b). The technique has been applied to many types of atmospheric phenomena (Hillger and Ellrod 2000, 2002, manuscript submitted to *J. Appl. Meteor.*). In addition, the use of PCA becomes increasingly important as the number of spectral bands increases, as is happening in atmospheric remote sensing. The mechanics of the PCI technique (see Web site www.cira.colostate.edu/ramm/cal_val/pci.htm) as applied to satellite imagery appear in the appendix.

Satellite imagery may be displayed in several different measurement units. The most basic units are scaled counts (12-bit counts ranging from 0 to 4095 for MODIS), a nondimensional scale that has a fixed and linear scaling to radiance units measured directly by the satellite instrumentation. Other possible measurement units include radiances, and temperatures (for the infrared images) or albedos (for visible images). Radiances have a linear relationship with the scaled counts, but temperatures are nonlinearly related to radiances. In spite of these differences, PCIs created from scaled counts and those created from either radiances, infrared temperatures, or albedos are generally not significantly different. For that reason, and for basic simplicity, PCIs generated from the original scaled counts are used in this study.

Half-hourly GOES imagery is used by the Washington Volcanic Ash Advisory Center (VAAC) to routinely produce analyses of ash clouds. One of the image products used to generate the ash advisories is PCI analysis of GOES multispectral imagery. PCI analysis has been running operationally at the Washington VAAC since December 1999 and several product upgrades have been provided based on feedback from Satellite Analysis Branch (SAB) meteorologists. The basic PCI product is a three-band image based on the three infrared bands (bands 2, 4, and 5 at 3.9, 10.7, and 12.0 μm, respectively) of the GOES Imager. Each of the three component images is a linear combination of the input bands with weights applied based on a transformation of the bands using eigenvector/eigenvalue analysis of the original imagery. For the GOES Imager, the second and third principal components (PCI-2 and PCI-3) have proven to be the most useful for volcanic hot spot and ash cloud detection, respectively. This is because the common or correlated information in the three GOES infrared bands is relegated to PCI-1. PCI-2 and PCI-3 contain band-difference information that highlights features not seen in single-band imagery alone. PCI-2 is primarily a band-2/4 (shortwave/longwave difference) image, and PCI-3 is primarily a band-4/5 (longwave split-window difference) image, with small contributions from the remaining band in each case.

3. Daytime analysis of volcanic ash

The first case analyzed for this study was a large eruption of ash from Popocatepetl volcano (hereinafter abbreviated Popo; 19.02°N, 98.62°W) at 5465 m elevation near Mexico City. The volcano, after giving off occasional and limited ash emissions for the preceding 2 or 3 yr, became quite active again in late 2000. One of the days with widespread ash was 20 December 2000. Figure 1 shows an analysis issued by the Washington VAAC (1999) giving the extent of the ash cloud based on GOES multispectral imagery for 1715 UTC. This

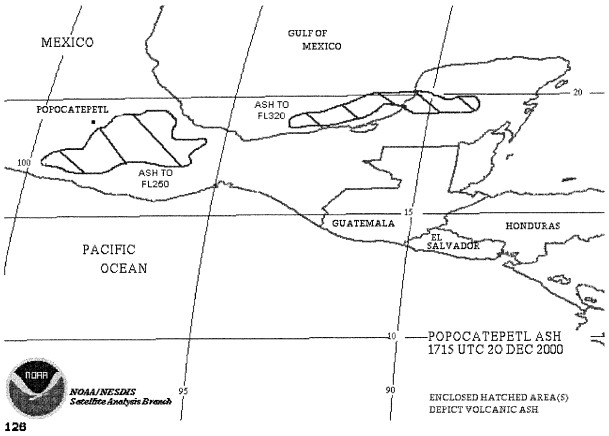

FIG. 1. Volcanic ash analysis at 1715 UTC (daytime) 20 Dec 2000 for Popocatepetl volcano near Mexico City. Analysis based on GOES multispectral imagery by the Satellite Analysis Branch (SAB) Washington VAAC.

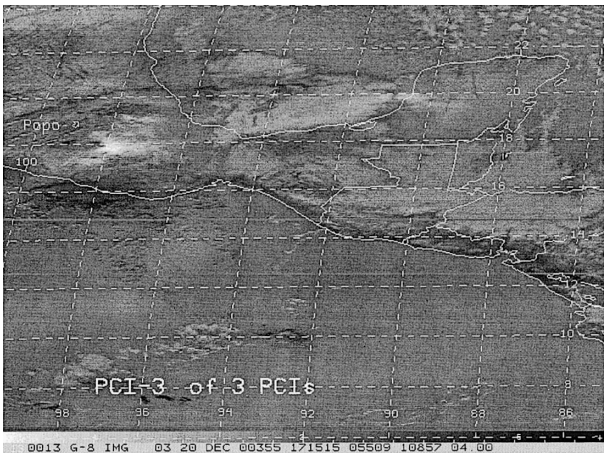

FIG. 2. PCI-3 of three PCIs that were generated from the three thermal infrared bands (2, 4, and 5) of GOES for 1715 UTC (daytime) 20 Dec 2000. PCI-3 is one of the products used to generate the ash analysis in Fig. 1. This product shows the ash cloud with significant contrast to the image background. This PCI is inverted black-to-white to make the ash cloud white.

analysis time matches the time of the MODIS imagery analyzed using PCIs. The ash extends mainly south and east of Popo, to as far east as the Yucatan Peninsula. In the analysis the ash is given in two parts, at different flight levels [FL250 (25 000 ft/7600 m) and FL320 (32 000 ft/9800 m)]. These levels were estimated by effectively matching the derived vector motion of the ash as seen in GOES imagery to the appropriate height levels from the Mexico City upper-air sounding and a model sounding.

Figure 2 is one of the GOES products used to generate the ash analysis in Fig. 1. PCI-3 is a three-band product, but is primarily a band-4/5 longwave split-window difference. Tracking of the ash over time, using half-hourly imagery, also helped to identify the extent of the ash cloud. This product shows the ash cloud with good contrast to the image background, but with somewhat limited contrast to some of the other image features. The ash signal is mainly to the east and southeast of Popo. Ash also extends further east to a secondary maximum over the Yucatan. The extent of the ash in both the ash analysis and PCI-3 serve as guides for the MODIS analysis to follow. However, the possibility of ash elsewhere should be mentioned since no current ash detection technique is infallible, and there is usually no independent confirmation that ash is present where the ash signals are seen in these images.

MODIS data for this volcanic ash case were available from the southbound pass of EOS *Terra* at 1715 UTC, a swath that covered most of Mexico. None of the MODIS bands showed the relatively diffuse ash for this case when viewed alone. This is expected when the ash signal is subtle, appearing in contrast to the image background much more readily in multiple-image combinations. Ash that is associated with meteorological cloud (composed primarily of water and ice droplets) can more easily be seen in single-band images, but the ash content may be unknown.

PCIs for this study were initially generated with MODIS data divided into two parts. The analysis was performed independently on the 19 visible/near-infrared (reflective) bands (1–19) and on the 17 longer-wavelength infrared (thermal) bands (20–36). (Band 26 at 1.38 μm is grouped with the longer-wavelength bands but is *not* in the thermal infrared portion of the spectrum.) The main reason for this division is a current limitation on the number of bands that can be analyzed with the PCI software being used. Analysis of the 19 visible/near-infrared bands did not result in any PCIs that show significant detection of the volcanic ash. Therefore the PCIs generated from the visible bands will not be discussed. However, the PCI analysis of the 17 MODIS thermal infrared bands provided several views of the ash cloud. Table 1 shows the bandwidths and primary uses of MODIS thermal infrared bands used in the analysis.

The PCI analysis of the 17 thermal infrared bands of MODIS resulted in 17 PCIs of varying information content. It is not necessary to explain the content of each PCI. Rather, this paper will discuss only those PCIs that qualitatively show significant evidence of ash in contrast to the image background and other image features. This will lead into an analysis of the MODIS bands that contributed to those PCIs. The MODIS data for this case are remapped from the polar-orbit projection into the GOES projection. Remapped MODIS images can be more easily compared and contrasted with the ash analysis in Fig. 1 and the GOES image in Fig. 2.

Figure 3, showing PCI-1, is given as a cloud reference image. PCI-1 contains by far the majority (76%) of the information content (explained variance) in the 17 MODIS bands that went into the 17 PCIs. This primary component contains information common to all the in-

TABLE 1. MODIS thermal infrared bands and bandwidths.

Primary use	MODIS band No.	Bandwidth (μm)
Surface/cloud temperature	20	3.66–3.84
(shortwave CO_2)	21	3.929–3.989
	22	3.929–3.989
	23	4.02–4.08
Atmospheric temperature	24	4.433–4.498
(shortwave CO_2)	25	4.482–4.549
Cirrus clouds	26*	1.36–1.39
Water vapor	27	6.535–6.895
	28	7.175–7.475
	29	8.4–8.7
Ozone (O_3)	30	9.58–9.88
Surface/cloud temperature	31	10.78–11.28
(window and "dirty" window)	32	11.77–12.27
Cloud-top altitude	33	13.185–13.485
(longwave CO_2)	34	13.485–13.785
	35	13.785–14.085
	36	14.085–14.385

* Band 26 at 1.38 μm included here is not in the thermal infrared portion of the spectrum.

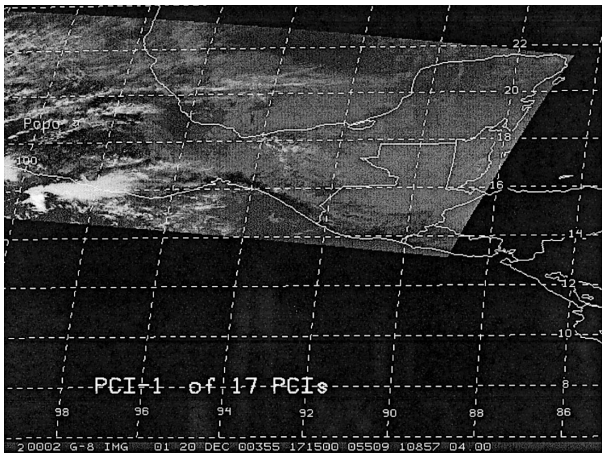

FIG. 3. PCI-1 of 17 PCIs that were generated from the 17 thermal infrared bands of MODIS for 1715 UTC (daytime) 20 Dec 2000. PCI-1 shows the main cloud features common to all of the MODIS infrared bands. The whitest areas are the highest clouds, low clouds are medium gray, and land surfaces are dark.

put bands. As such it gives an idea of the overall cloud conditions at the time of the event with the main features available in most of the thermal infrared bands. The highest clouds are the whitest areas, low clouds are medium gray, and land surfaces are dark. Land surfaces vary in temperature from the blackest (hottest) to lighter gray (cooler). The area around Popo (indicated by an arrow and a label) contains some middle- to higher-level clouds. The white features that appear in PCI-1, as a result of appearing in most of the infrared bands, are meteorological cloud. No ash cloud is apparent in this image. Rather, the ash appears in higher-numbered PCIs where it becomes detectable by combining images from various spectral regions.

a. Analysis of the PCIs that show ash

Of the remaining higher-numbered PCIs, only those in which ash was detected with significant contrast to the image background and other image features will be discussed. The discussion will focus on where the ash was detected in each PCI, some of the relative qualities of those images for ash detection, and finally on the MODIS bands that contributed to those PCIs.

Table 2 summarizes 9 (of 17) PCIs that contained an identifiable ash signal. The PCIs are listed in order of decreasing ash signal or contrast to the image background and other image features. In PCI-9, -8, and -16 the ash has much more contrast to surrounding regions than in PCI-14, -4, and -10, and even more contrast than in PCI-13, -15, and -7, which are of limited value for ash detection.

The relative qualities of each PCI are given in the second column of Table 2. Detection problems, such as low contrast, noise, and confusion between ash cloud and nonash features, are noted. Because of the decreasing ability to detect ash compared to the image background and other image features, it is increasingly hard to use more than the first six PCIs in Table 2 to determine the presence of ash for this case. Only the first four PCIs, three of them showing the ash cloud well and one with lesser ability to detect ash, will be discussed.

Each PCI consists of combinations of all input bands, but only a few of the original bands contribute heavily to the PCIs. Typically those few bands stand out from the others by their much larger weight in the creation of the PCIs. The last two columns of Table 2 contain the percentage of the explained variance and the signal-to-noise ratio (SNR) for each PCI. The SNRs were determined using spatial structure analysis (Hillger and

TABLE 2. PCIs in descending order of qualitative value for ash cloud detection (Popo daytime case).

PCI No.	Qualitative assessment of ash contrast	PCI explained variance (%)	SNR
9	Good ash signal	0.12	1.70
8	Good ash signal, noisy	0.18	1.26
16	Good ash signal, but cloud contamination	0.002	3.30
14	Densest ash only, low contrast	0.012	1.48
4	Densest ash only, significant cloud contamination	2.7	6.55
10	Densest ash only, low contrast, noisy	0.07	1.26
13	Very weak, low contrast	0.027	1.20
15	Very weak, contaminated	0.003	1.70
7	Questionable value	0.39	3.71

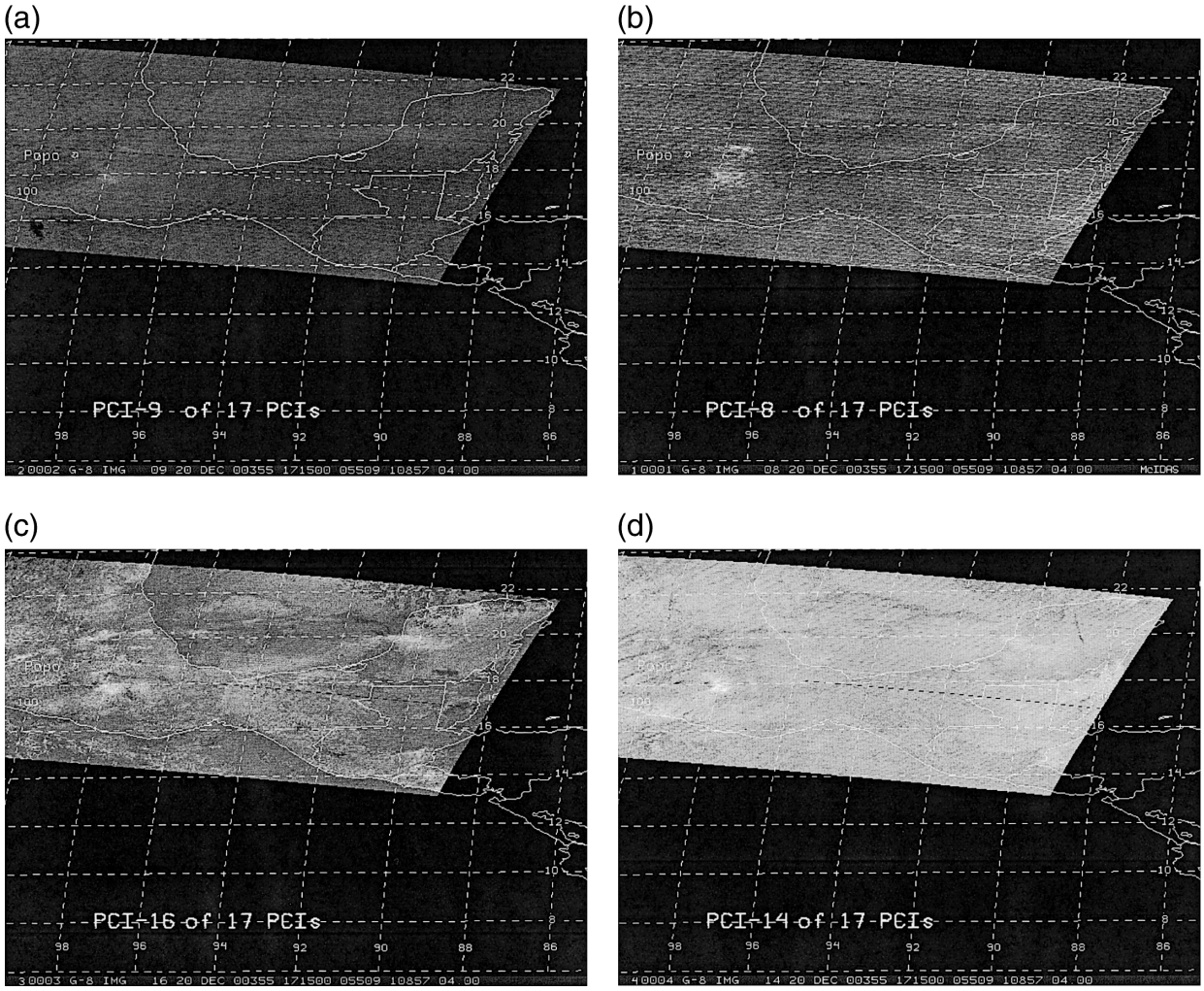

FIG. 4. (a) PCI-9 of 17 PCIs that were generated from the 17 thermal infrared bands of MODIS for 1715 UTC (daytime) 20 Dec 2000. PCI-9 shows the ash cloud as light gray, with good contrast to the image background and low noise. (b) Same as in (a) but for PCI-8. PCI-8 shows the ash (white) but contains significant image striping and noise from the MODIS instrument as compared with PCI-9. (c) Same as in (a) but for PCI-16. PCI-16 shows the ash cloud as lighter gray, but suffers from possible false ash signals due to cloud contamination. (d) Same as in (a) but for PCI-14. PCI-14 shows mainly the densest parts of the ash cloud (white).

Vonder Haar 1988). An SNR greater than 1.0 implies sufficient signal in the image to view features (e.g., a ratio of 1.70 means there is 70% more signal than noise in that PCI). These two columns show that the information content of the PCIs is a very small fraction of the total signal in the MODIS bands, and that the signal in some of the PCIs is only marginally above the noise level of the image. From these numbers it is clear that the best ash signal does not necessarily come from PCIs with larger explained variances or higher SNRs.

PCI-9 in Fig. 4a shows the volcanic ash as light gray in contrast to the image background. The ash also appears in PCI-8 in Fig. 4b but with more noise than PCI-9. Table 2 gives an SNR of 1.70 for PCI-9 and 1.26 for PCI-8. The SNR is quite small for both PCIs, but there is sufficient signal above noise and contrast to the image background that the extent of the ash in both of these PCIs agrees well with the ash analysis (Fig. 1). However, the increased signal-to-noise ratio for PCI-9 gives the image a smoother-looking background, as opposed to the more apparent noise and line-to-line striping (due to multiple detectors in the MODIS instrument) in PCI-8. (There is also one bad half-line of data near the middle of the MODIS band-30 image that was transferred into most of the PCIs as a dashed line similar to the latitude and longitude lines.)

In PCI-8 the portion of the volcanic ash not obscured by the clouds, as identified in PCI-1 (Fig. 3), is denser to the east and southeast of Popo. The ash also extends quite far east over the Yucatan Peninsula, where there is a secondary maximum due to an earlier exhalation of ash. The elongated west–east area of ash extending to the Yucatan may be slightly easier to identify in PCI-8 than in PCI-9, but there is increased chance of con-

TABLE 3. MODIS bands contributing heavily to the first six PCIs in Table 2 (in descending order of ash cloud contrast to the image background and other image features). Negative values are in parentheses. Boldface values are explained in text.

	Explained variance and sign of MODIS bands								
PCI	20 3.75 μm	25 4.52 μm	29 8.6 μm	30 9.7 μm	31 11.0 μm	32 12.0 μm	33 13.3 μm	34 13.6 μm	36 14.2 μm
9	3%	(11%)	(~0%)	**51%**	~0%	(~0%)	1%	1%	**(16%)**
8	4%	**(19%)**	2%	9%	1%	~0%	(2%)	(6%)	**54%**
16	~0%	~0%	(7%)	(~0%)	**63%**	**(17%)**	(~0%)	~0%	~0%
Sum of above	7%	**30%**	9%	**60%**	**64%**	17%	3%	7%	**70%**
14	1%	(2%)	**48%**	(4%)	(2%)	**(36%)**	1%	~0%	(~0%)
4	**24%**	1%	**(17%)**	(1%)	(6%)	(6%)	~0%	6%	12%
10	(1%)	(1%)	1%	~0%	~0%	(1%)	**(36%)**	**43%**	(1%)
Sum of all above	33%	34%	**75%**	**65%**	**72%**	**60%**	40%	**56%**	**84%**

fusion between ash and the low clouds to the south seen in PCI-1. Also, another difference between the two PCIs is that the maximum ash signal is east of Popo in PCI-8 and more southeast of Popo in PCI-9, probably due to variations in the height of the ash as noted in the analysis.

Figure 4c shows PCI-16, the next PCI in Table 2, with somewhat reduced ability to detect ash. The extent of the ash in PCI-16 is quite similar to that of GOES PCI-3 in Fig. 2. PCI-16 is interesting because there is more connection between the primary ash maximum near Popo and the secondary ash maximum over the Yucatan, highlighting this portion of the ash cloud. The secondary maximum also appears more intense than in either PCI-9 or PCI-8. The variations are likely due to changes in the ash particle concentration and height of the ash in various parts of the cloud. PCI-16 also contains more false ashlike signals. In particular, the thin line of ashlike signal just north of Popo, stretching from the western edge of the image eastward to 95°W, is identifiable as cirrus in PCI-1. Nonash contamination of the signal can cause misidentification and either over- or underestimation of the extent of the volcanic ash. This nonash signal is probably the source of the increased signal-to-noise ratio (3.3 from Table 2) in PCI-16, not the ash signal.

The ash cloud is manifest to a lesser extent in the next three PCIs: PCI-14, PCI-4, and PCI-10. Only the first of these PCIs is shown (Fig. 4d), representative of the decreasing ability of further PCIs to identify the ash compared to other features in the images. In PCI-14 (Fig. 4d) the ash signal is concentrated at two ash maxima only, one directly southeast of Popo and the other to the east over the Yucatan. The lower contrast of the ash signal to the image background highlights the ash in the maxima, indicating where the ash particle concentration is the greatest, with little ash seen between the two maxima. Cloud contamination is less of a problem with PCI-14 than PCI-16.

Although at least two of the remaining PCIs show portions of the ash cloud, the contrast between the ash and the surrounding background regions is low and cloud contamination increases. For these PCIs, when the signal becomes weak, approaching the limits of detection, there is an increased possibility of false detection of ash. Although PCI-4 (not shown) has a much larger SNR (from Table 2) than the other PCIs, that signal above noise is due to significant cloud contamination.

Table 3 gives information on the MODIS bands that contributed the most to the PCIs that were best at detecting the ash cloud. Only the nine MODIS bands that contributed significantly to the first six PCIs in Table 2 are listed. For each of those bands the explained variance and sign are given for their contribution to each of the PCIs. The explained variance is a measure of the magnitude of the contribution of each band and the sign is given to indicate whether the band contributed positively or negatively to a particular PCI. Whether the sign of a particular band is positive or negative is only important relative to the signs of the other bands, otherwise any PCI can be inverted along with the signs of all of the bands that contributed to it.

In Table 3 the bands with the most positive and the most negative explained variance are shown in bold for each PCI. The row following the first three PCIs in the table contains the sums of the explained variances for each band to the first three PCIs, regardless of the sign of the contribution. The bands that are considered most important for volcanic ash detection, with summed variances over 30%, are shown in bold. In this case the most important bands for overall ash detection are 36, 31, 30 (in decreasing significance) and 25 (marginally). Likewise, the final row in Table 3 gives the sums of the explained variances for each band in all six PCIs indicated as adequate for ash detection. This time, the most important bands—with summed variance over 50%—are bands 29–32, 34, and 36. The additional bands (29, 32, and 34) are important for locating more subtle variations in ash cloud density, such as seen in PCI-14. Thus these bands should not be excluded from ash analysis if they are available.

The bands determined to be most important combine in various ways to reveal the ash: PCI-9 is the difference between the ozone and longwave CO_2 bands (9.7 and 14.2 μm, respectively); PCI-8 is mainly the difference

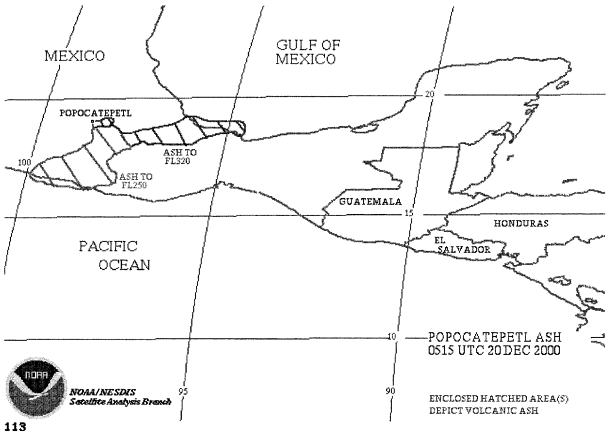

FIG. 5. Volcanic ash analysis at 0515 UTC (nighttime) on 20 Dec 2000 for Popocatepetl volcano near Mexico City. Analysis based on GOES multispectral imagery by the Satellite Analysis Branch (SAB) Washington VAAC.

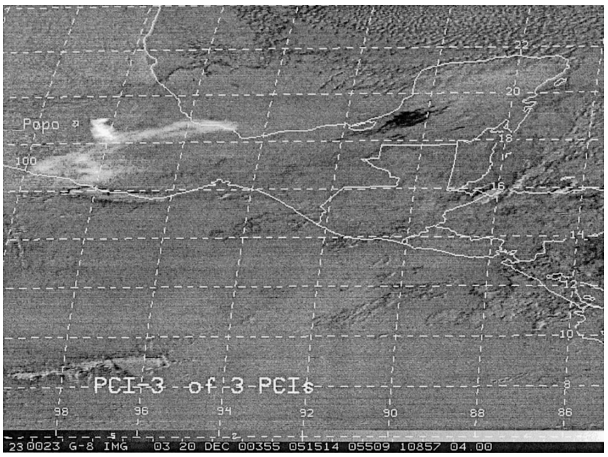

FIG. 6. PCI-3 of three PCIs that were generated from the GOES infrared bands 2, 4, and 5 at 0505 UTC (nighttime) 20 Dec 2000. PCI-3 is one of the products used to generate the ash analysis in Fig. 5. This product shows the ash cloud (white) with significant contrast to the image background.

between shortwave and longwave CO_2 bands (4.52 and 14.2 μm, respectively); PCI-16 is the difference between a longwave window band and a nearby ''dirty'' window band (11.0 and 12.0 μm, respectively); and PCI-14 is primarily the difference between a water vapor band and a dirty window band (8.6 and 12.0 μm, respectively).

There is an emissivity minimum between 8.0 and 9.7 μm due to silicate rock, which is probably why PCI-9 (a combination of bands 29 and 36) is most important. Also, band 29 at 8.6 μm is near the peak absorption for sulphate aerosol around 8.4 μm and is a weak SO_2 band (Prata 1989; Prata and Grant 2001), which is probably why the combination of bands in PCI-14 is important, in addition to the minimum in emissivity due to silicate in that portion of the spectrum.

With the multitude of bands available on MODIS, it is possible that different PCIs are better for ash detection in different situations. Additional cases that show this to be true will be examined.

b. MODIS detection of volcanic ash at night

The 20 December 2000 eruption of Popo was captured during a nighttime swath of MODIS data at 0505 UTC, about 12 h earlier than the daytime case already examined. Figure 5 shows the operational ash analysis for this second case. As in Fig. 1, the analysis of the ash cloud is given in two parts, at different flight levels [FL250 (25 000 ft/7600 m) and FL320 (32 000 ft/9800 m)].

Figure 6 shows PCI-3 generated from GOES bands 2, 4, and 5 at 0515 UTC. As in the daytime case, this is the only one of the three GOES PCIs that shows the ash cloud. In PCI-3 the ash cloud is clearly spread both to the south and east of Popo. The extent of the ash in both the ash analysis and PCI-3 serve as guides for the MODIS analysis to follow.

For nighttime situations, the lack of solar radiation changes the character of the signal in the MODIS shortwave infrared bands, which normally have a reflected component during the daytime. Those differences are manifest in the PCIs as expected in the analysis of this nighttime case compared to the daytime case.

PCIs were generated at night from the same subset of 17 MODIS infrared bands used for the daytime case. All of the images have been remapped into the GOES projection in Fig. 6. Figure 7 shows PCI-1, which contains information on the overall cloud situation. There is very little cloud near Popo at this time. The only major feature is an elongated patch of clouds on the coast of Mexico south of Popo.

Table 4 lists the characteristics of the PCIs that detected the ash cloud most clearly, in order of decreasing contrast of the ash to the image background and other image features. As in Table 2, the positive and negative qualities of each PCI are listed in the second column. The explained variance and SNR of the PCIs are given in the last two columns of the table. From these numbers it is again clear that the best ash signal is not necessarily seen in PCIs with larger explained variances or higher SNRs.

The first six PCIs in Table 4 detected the ash cloud from Popo well at night, with the first three (PCI-7, -8, and -13) being the best, and the next three (PCI-15, -5, and -4) of lesser value. The last three PCIs (PCI-10, -12, and -6) in Table 4 are of limited value. It should also be noted that some of the PCIs are inverted black-to-white so that the ash cloud appears white in all of the images. This scale inversion is equivalent to changing the signs of all the bands that contribute to a PCI. Only the first six PCIs in Table 4 will be shown and discussed, in order of decreasing contrast of the ash cloud to the image background.

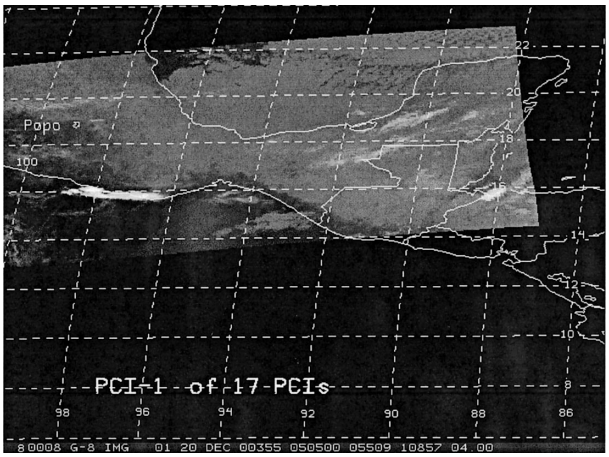

FIG. 7. PCI-1 of 17 PCIs that were generated from the 17 thermal infrared bands of MODIS for 0505 UTC (nighttime) 20 Dec 2000. PCI-1 shows the main cloud features common to all of the MODIS infrared bands.

TABLE 4. PCIs in descending order of qualitative value for ash cloud detection (Popo nighttime case).

PCI No.	Qualitative assessment of ash contrast	Explained variance (%)	SNR
7	Good ash signal	0.088	2.20
8	Good ash signal, but low-level cloud contamination	0.055	2.67
13	Good ash signal, some contamination	0.005	2.00
15	Densest ash only, some contamination	0.001	2.15
5	Densest ash only, cloud contamination	0.53	3.67
4	Densest ash only, significant cloud contamination	1.2	5.21
10	Very weak, contaminated	0.015	1.83
12	Very weak, low contrast	0.008	1.64
6	Questionable value	0.17	2.03

PCI-7 and PCI-8, in Figs. 8a and 8b, respectively, show the ash cloud as densest near Popo, somewhat similarly to GOES PCI-3 in Fig. 6. The main part of the ash cloud to the east is connected to the volcano, but another more diffuse part of the ash cloud to the south is disconnected from the main cloud. PCI-8 differs from PCI-7 in that some cloud along the coast of Mexico south of Popo also appears white and contaminates the ash signal in PCI-8. Another difference is that PCI-8 shows a slight connection between the main ash cloud east of Popo and the ash cloud to the southeast of Popo, as indicated in the ash analyses (Fig. 5). This connection is not as clear in PCI-7, probably due to its lower signal-to-noise than PCI-8 (Table 4).

PCI-13 and PCI-15, in Figs. 8c and 8d, respectively, show similarly shaped ash signals, but with less contrast to the image background than PCI-7 and -8. Because of this lower contrast, confusion between ash and other cloud signals is possible using PCI-13 and -15. Note also that the lower-level ash area to the southwest of Popo, as given in the ash analysis (Fig. 5), is less obvious than in PCI-7 and -8.

Last, PCI-5 and PCI-4, in Figs. 8e and 8f, respectively, show mainly the part of the ash cloud connected to Popo, in contrast to the four PCIs already discussed, which showed additional ash to the south of Popo. PCI-5 and -4 increasingly contain areas of false signal that could be confused with ash if these images were used in isolation. Note in particular the possible northward extension of the ash from the main west–east part of the ash cloud in PCI-5. It is doubtful that this area is really ash, as it appears only in this PCI and no others.

Table 5 is provided to give additional information on the MODIS bands that contributed the most to the ash-detecting PCIs using nighttime data. In this case the input to the first six PCIs in Table 4 comes primarily from combinations of 10 of the 17 MODIS thermal bands. Data are presented as in Table 3.

The sums of the explained variances for the first three PCIs in Table 5, with values above 30%, are shown in bold, indicating that MODIS bands 22, 29, 30, and 34 are of most significance. Then, when the variances of the bands for the next three PCIs are added, bands 27 and 30–32 (from the water vapor, ozone, and longwave CO_2 portions of the spectrum) are most significant, with a summed variance of 50% or greater. This is a big change in the most-significant bands, adding three and dropping three of the bands that were most significant to the first three PCIs. Unlike the daytime case, band 29 (8.6 μm) does not appear among the bands of most significance in this nighttime case, although it has significance for the first three PCIs.

The MODIS bands combine in various ways to reveal the ash: PCI-7 is mainly the difference between a longwave CO_2 band (13.6 μm) and the ozone band (9.7 μm); PCI-8 is the difference between the ozone band and a shortwave CO_2 band (4.52 μm); PCI-13 is the difference between a shortwave CO_2 band (3.96 μm) and a lower-level water vapor band (8.6 μm); PCI-15 is the split-window difference between the 11- and 12-μm bands; PCI-5 is mainly the difference between the midlevel water vapor (and SO_2) band (Prata 1989; Prata and Grant 2001) at 7.3 μm and the upper-level water vapor band (6.7 μm); and finally, PCI-4 is the difference between the upper-level water vapor band (6.7 μm) and a longwave CO_2 band (13.3 μm). Again, the 7.3- and 9.7-μm bands, situated in the spectral region known for volcanic cloud signals, are important bands in combination with bands outside this region.

As in the daytime case, several of the bands contributed significantly (larger summed variances) to only one or two of the PCIs. A different subset of the MODIS

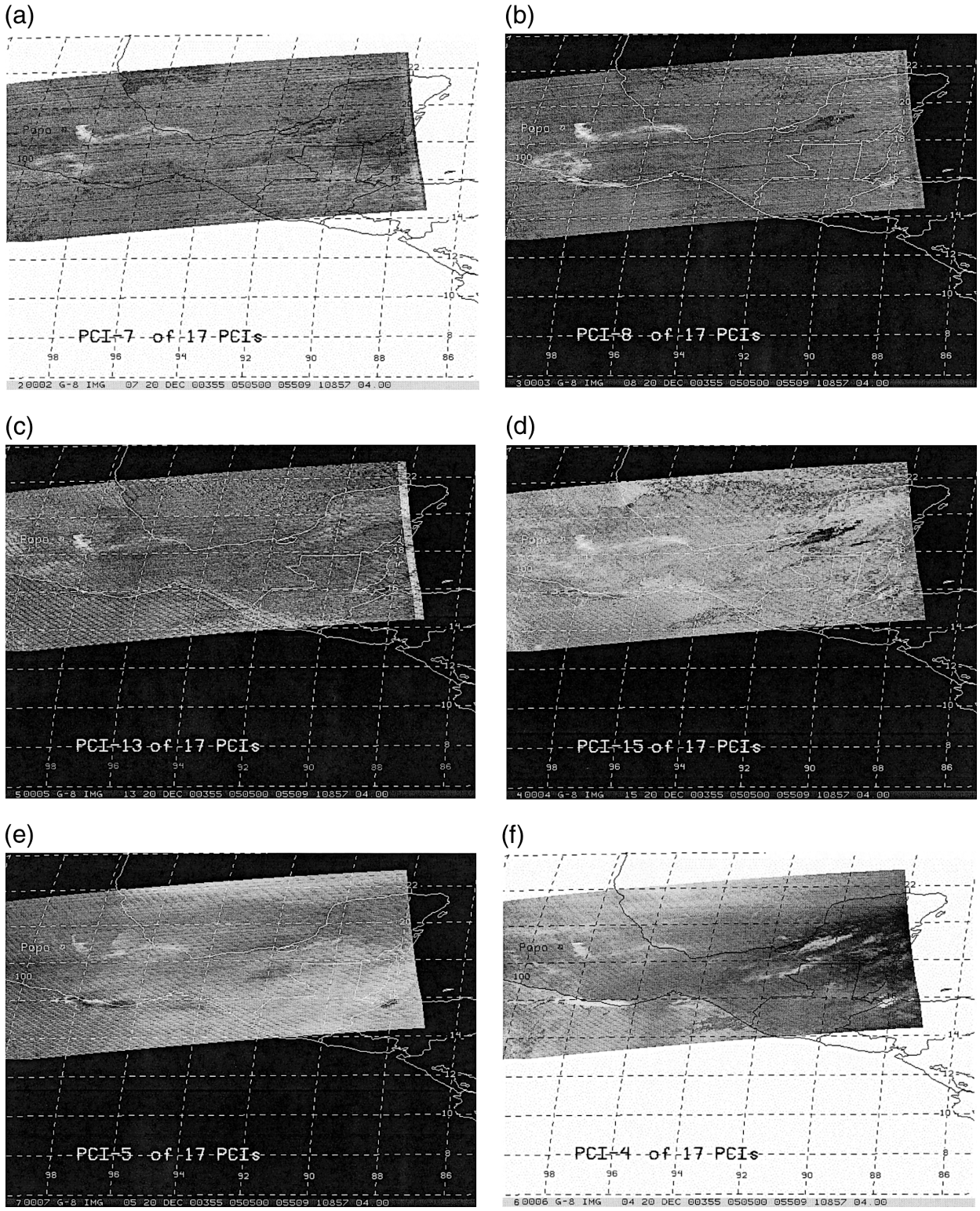

FIG. 8. (a) PCI-7 of 17 PCIs that were generated from the 17 thermal infrared bands of MODIS for 0505 UTC (nighttime) 20 Dec 2000. PCI-7 shows the ash cloud (white). This PCI is inverted black-to-white to make the ash cloud white. (b) Same as in (a) but for PCI-8. PCI-8 shows the ash cloud (white), as in PCI-7, but with false ash signals from the cloud along the coast of Mexico south of Popo. (c) Same as in (a) but for PCI-13. PCI-13 shows the ash cloud (white), but with increased noise and cloud contamination. (d) Same as in (a) but for PCI-15. PCI-15 shows the ash cloud at the higher levels better than the lower-level ash. (e) Same as in (a) but for PCI-5. PCI-5 again shows the ash cloud at the higher levels better than the lower-level ash. (f) Same as in (a) but for PCI-4. PCI-4 shows the densest parts of the ash cloud, again with false ash signals from clouds. This PCI is inverted black-to-white to make the ash cloud white.

TABLE 5. MODIS bands contributing heavily to the first six PCIs in Table 4 (in descending order of ash cloud contrast to the image background and other image features). Negative values are in parentheses. Boldface values are explained in text.

	Explained variance and sign of MODIS bands									
PCI	22 3.96 μm	25 4.52 μm	27 6.7 μm	28 7.3 μm	29 8.6 μm	30 9.7 μm	31 11.0 μm	32 12.0 μm	33 13.3 μm	34 13.6 μm
7	7%	(~0%)	~0%	(~0%)	(11%)	**(23%)**	(2%)	(~0%)	2%	**25%**
8	~0%	**(23%)**	(~0%)	(~0%)	2%	**32%**	(~0%)	(10%)	(8%)	17%
13	**(27%)**	(3%)	(~0%)	~0%	**(19%)**	3%	15%	2%	~0%	(~0%)
Sum of above	**34%**	26%	0%	0%	**32%**	**58%**	17%	12%	10%	**42%**
15	(1%)	1%	0%	(~0%)	~0%	(3%)	**46%**	**(38%)**	~0%	0%
5	(~0%)	5%	**(31%)**	**39%**	(1%)	1%	(5%)	(4%)	(2%)	(1%)
4	5%	4%	**27%**	(1%)	(8%)	1%	(8%)	(11%)	**(15%)**	(2%)
Sum of all above	40%	36%	**58%**	40%	41%	**63%**	**76%**	**65%**	27%	45%

bands were found most significant at night compared to the daytime case. The bands in common with the daytime case are bands 30, 31, and 32, which include the longwave split-window bands (11 and 12 μm). Other bands contribute to detection of volcanic ash, but with lower explained variances; these bands add information about variations in ash (and gas) particle concentration and height. The MODIS bands not listed in the tables, which have the lowest summed variances, appear to be the least important for ash detection.

4. Additional volcano cases

Two additional cases are presented, this time for a volcano in a different part of the world, to add strength to the cases already examined for this study of volcanic detection using MODIS. MODIS data were obtained for both day and night cases with a significant amount of ash from Cleveland volcano in Alaska. Mount Cleveland is on Chuginadak Island in the Aleutian Island chain (52.49°N, 169.57°W) at 1730-m elevation. An eruption started at approximately 1400 UTC on 19 February 2001. For both of these cases neither the Washington nor Alaskan VAACs generated ash analyses. Therefore there is no need to remap the MODIS data to match those analyses. Rather, the MODIS images are presented directly in their polar-orbit projections based on scan lines taken along the orbit track (at 1- and 2-km spatial resolution for the day and night cases, respectively). The night case is presented before the day case, as the results are more similar to the Popo cases already examined.

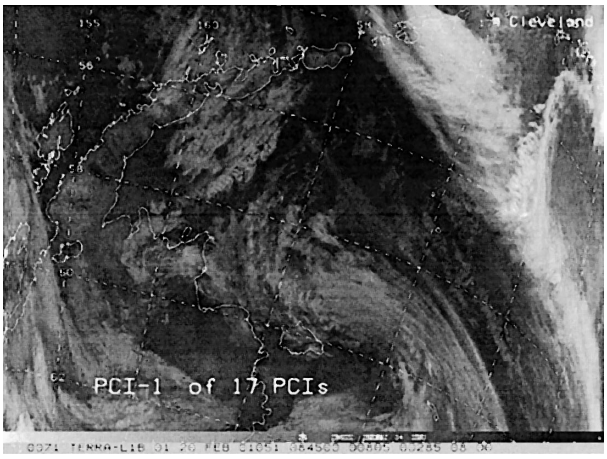

FIG. 9. PCI-1 of 17 PCIs that were generated from the 17 thermal infrared bands of MODIS at 0845 UTC (nighttime) 20 Feb 2001 for Cleveland volcano in the Aleutian Islands. PCI-1 shows the main cloud features common to all of the MODIS infrared bands.

Figure 9 is PCI-1 of 17 PCIs for the nighttime Cleveland case, at 0845 UTC on 20 February 2001, almost 19 h after the eruption. The MODIS orbit from south to north gives a rotated (north at the bottom) view of the area surrounding this volcano. PCI-1 only minimally shows the volcanic ash, which becomes much more apparent in the subsequent PCIs. Rather, PCI-1 shows both high clouds (white) and low clouds (light gray), features that appear in most of the MODIS infrared bands.

Table 6, organized like Tables 2 and 4, lists the PCIs that show the Cleveland ash to a significant degree. Only 7 (of 17) PCIs that contained identifiable ash are listed, with the first 5 being much better for ash detection than the last 2. Of those five, the first three PCIs (6, 12, and 11) are by far the best at detecting the extent of the ash cloud. The next two PCIs (8 and 13) highlight differences between the denser and the more diffuse parts of the ash cloud. Below, we examine some of the more important PCIs in more detail.

Figures 10a,b,c show PCI-6, -12, and -11, respectively, with good indications of ash signal. At this time Cleveland was no longer emitting ash. Rather, the ash cloud (which ranges from white to light gray) was detached from the volcano (indicated by an arrow and a label, near the upper-right corner of the figure) and the ash was being carried by the prevailing winds to the east and far north (to the left and down in the figure). The ash cloud, which is over 1000 km long, seems to extend off the bottom of the image. However, the ash merges northwards with a similar-looking elongated cloud feature seen in PCI-1 (Fig. 9).

In contrast to the first three PCIs already discussed, PCI-8 in Fig. 10d shows only the densest portion of the

TABLE 6. PCIs in descending order of qualitative value for ash cloud detection (Cleveland nighttime case).

PCI No.	Qualitative assessment of ash contrast	Explained variance (%)	SNR
6	Good ash signal	0.18	1.65
12	Good ash signal, noisy	0.017	2.09
11	Good ash signal, but cloud contamination	0.022	1.21
8	Densest ash only, lower contrast	0.091	2.03
13	More diffuse ash only, significant cloud contamination	0.002	2.88
10	Very weak, low contrast	0.037	1.65
7	Very weak, low contrast	0.11	1.61

ash cloud, and PCI-13 in Fig. 10e misses the densest ash, showing only the more diffuse ash to the northwest (down in the figure).

Table 7 summarizes the MODIS bands that contributed significantly to the first five PCIs in Table 6. As in Tables 3 and 5, the explained variances are summed for two groups of PCIs: those showing the ash best, and those with less overall ash signal, but with important variations in the ash cloud density and/or height of the ash. Summed variances over 30% and over 50%, respectively are bolded. The bottom line in Table 7 indicates that MODIS bands 24, 25, and 28–32 are the most important. This differs somewhat from the results for ash detection from the two Popo cases, but includes the longwave bands 30–32 (9.7–12.0 μm), the bands found of most value both by day and night. However, of equal importance are bands 24 and 25 (around 4.5 μm) in the shortwave portion of the spectrum, and bands 28 and 29 (7.3 and 8.6 μm, respectively) in the water vapor (and SO_2) spectrum. The 7.3–9.7-μm bands are in the portion of the spectrum with significant silicate particle and sulphate aerosol absorption, and SO_2 gas.

Next, we examine the daytime case for the Cleveland volcano at 2310 UTC on 20 February 2001, about 9 h after the eruption. Figure 11 shows PCI-1 of 17 PCIs, with a large arc of meteorological cloud being carried by winds to the east and north of Cleveland (indicated by an arrow and a label). The potential ash components of this cloud will be revealed only in higher-numbered PCIs. In this case the MODIS pass is from north to south, without the rotated view of the nighttime Cleveland case.

What is different about this case, when compared with the others already examined, is the large amount of meteorological (water/steam/ice-rich) cloud apparently associated with the Cleveland eruption at this time. Since clouds in general are opaque to the infrared bands, this cloud signature appears in all of the MODIS bands and therefore in nearly every PCI, including PCI-1. When ash is mixed with the meteorological cloud, the cloud can mask parts of the ash, unlike the Popo cases where little meteorological cloud contaminated the multispectral analysis.

The PCIs in Table 8 are arranged similarly to Tables 2, 4, and 6, in decreasing order of relative value for ash detection. However, because of the large meteorological cloud signal, which appears in nearly every PCI, only those PCIs in which the cloud looks different than in PCI-1 are listed. The first four PCIs in Table 8 show the ash extending up to 300 km farther downwind to the northwest, and the next four PCIs show distinct changes in the image from black for the denser part of the volcanic cloud (presumably a water-rich portion of the volcanic cloud based on nearly identical signatures in the MODIS infrared bands), to white for the more diffuse part of the volcanic cloud (presumably ash due to differential signatures among the MODIS infrared bands).

Figure 12a shows PCI-5, as representative of the first four PCIs in Table 8 with ash cloud extending the farthest downwind. In this and the next three PCIs (not shown) the ash cloud ranges from white to light gray. Ash is being carried by winds to the east and north (to the right and continuing in a curve extending up and to the left) of Cleveland (indicated by an arrow and a label). In the three PCIs not shown (7, 4, and 14), the ash appears with a similar shape, but with decreasing contrast to the image background and increased contamination by other image features. Figures 12b and 12c show PCI-16 and PCI-8, respectively, where there is a change from black to white across the volcanic cloud, between the denser water/steam/ice-rich part of the cloud seen in PCI-1 (Fig. 11), and the more diffuse part of the cloud. Note the different extents of the black and white portions in the two PCIs, indicating changes in ash cloud composition downwind. Although details of the ash cloud are not quantified, this change in enhancement is a good indication of changes in characteristics of the ash cloud such as decreasing H_2O/ash/SO_2 content, becoming more diffuse, or reaching a different height.

Table 9 shows the contributions of the MODIS bands to the PCIs for the Cleveland daytime case. In this case nearly all (15 of 17) of the MODIS bands contributed to a significant degree to the first six PCIs in Table 8. Variances over 30% in the first sum indicate that bands 24, 26, 29, 30, 34, and 36 are most important. However, when the explained variances for the next two PCIs are added to those for the first four PCIs, only a few of the bands contribute significantly to the ash-detecting PCIs. The most important bands, with summed variances over 50%, are now 26, and 28–32. (Band 26 at 1.38 μm with its ability to detect thin cirrus is the most important band in this particular case. So, it is possible that other PCIs computed from the visible/near-infrared MODIS

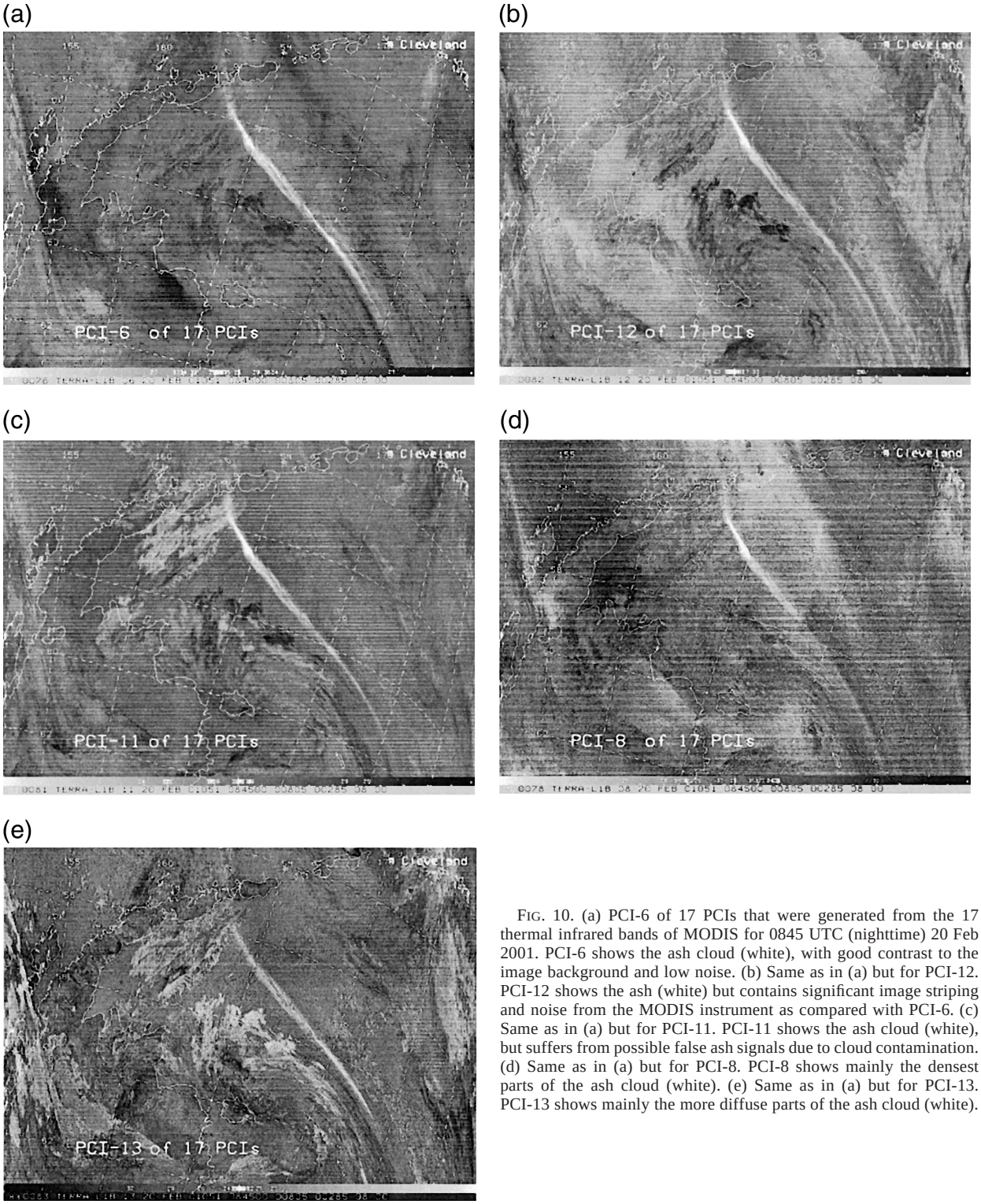

FIG. 10. (a) PCI-6 of 17 PCIs that were generated from the 17 thermal infrared bands of MODIS for 0845 UTC (nighttime) 20 Feb 2001. PCI-6 shows the ash cloud (white), with good contrast to the image background and low noise. (b) Same as in (a) but for PCI-12. PCI-12 shows the ash (white) but contains significant image striping and noise from the MODIS instrument as compared with PCI-6. (c) Same as in (a) but for PCI-11. PCI-11 shows the ash cloud (white), but suffers from possible false ash signals due to cloud contamination. (d) Same as in (a) but for PCI-8. PCI-8 shows mainly the densest parts of the ash cloud (white). (e) Same as in (a) but for PCI-13. PCI-13 shows mainly the more diffuse parts of the ash cloud (white).

bands might contain details of the ash cloud, but in general those PCIs appeared to show mainly variations in the water/ice cloud structure.) Among the bands greatly increased in importance are the split-window bands 31 and 32 (11 and 12 μm, respectively) and water vapor and SO_2 band 28 (7.3 μm). These are the bands that add distinction between the more-dense meteorological cloud and less-dense ash cloud.

TABLE 7. MODIS bands contributing heavily to the first five PCIs in Table 6 (in descending order of ash cloud contrast to the image background and other image features). Negative values are in parentheses. Boldface values are explained in text.

	Explained variance and sign of MODIS bands									
PCI	20 3.75 μm	22 3.96 μm	24 4.47 μm	25 4.52 μm	27 6.7 μm	28 7.3 μm	29 8.6 μm	30 9.7 μm	31 11.0 μm	32 12.0 μm
6	(0.6%)	(1.2%)	2.4%	(0.5%)	**(12.9%)**	**42.2%**	(0.6%)	**20.1%**	(0.9%)	(3.6%)
12	(~0%)	(0.1%)	**28.5%**	(12.2%)	0.2%	(1.2%)	**29.2%**	(7.5%)	0.1%	**(19.4%)**
11	(9.2%)	(8.5%)	**(16.8%)**	**30.0%**	0.1%	(0.8%)	**20.4%**	~0%	(1.5%)	9.5%
Sum of above	9.8%	9.8%	**47.7%**	**42.7%**	13.2%	**44.2%**	**50.2%**	27.6%	2.5%	**32.5%**
8	(2.4%)	(3.6%)	(4.6%)	**(21.5%)**	1.7%	(9.1%)	3.2%	**35.9%**	3.5%	1.0%
13	(2.9%)	0.3%	(0.3%)	0.7%	(~0%)	0.1%	(8.4%)	~0%	**63.7%**	**(21.5%)**
Sum of all above	15.1%	13.7%	**52.6%**	**64.9%**	14.9%	**53.4%**	**61.8%**	**63.5%**	**69.7%**	**55.0%**

5. Implications for future GOES Imager products

Current operational satellite instruments such as GOES do not contain as many bands or cover as many spectral regions as MODIS. This means that products developed for volcanic ash detection need to rely on far fewer spectral bands than are available in this study. In particular, the longwave split-window bands of MODIS, bands 31 and 32, which are also the ones most important for current GOES ash detection techniques, are among the MODIS bands there are best at detecting ash in all four volcanic cases examined. However, the split-window bands are not necessarily of greater importance than the ozone band 30 (9.7 μm) that contributed strongly to each case examined. Bands 28 and 29 (7.3 and 8.6 μm, respectively), in the water vapor and SO_2 spectrum, also contributed significantly to the first few PCIs in three of the four cases examined. In addition, other MODIS bands in the shorter and longer wavelength portions of the spectrum were of importance, in at least one of the volcanic cases, for distinguishing between ash and false ash signals that are sometimes associated with meteorological clouds.

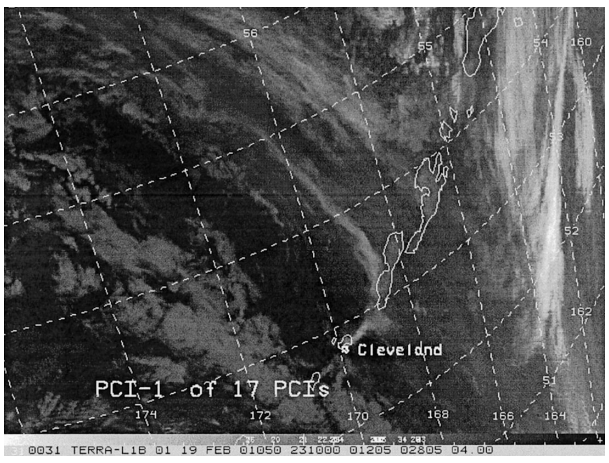

FIG. 11. PCI-1 of 17 PCIs that were generated from the 17 thermal infrared bands of MODIS at 2310 UTC (daytime) 20 Feb 2001 for Cleveland volcano in the Aleutian Islands. PCI-1 shows the main cloud features common to all of the MODIS infrared bands.

The MODIS bands indicated as preferential for volcanic ash detection can be used to help guide the development of new image products as additional bands become available. The next-generation GOES Imager, first scheduled for launch in 2012 as GOES-R, will contain many more bands than the current GOES Imager. Table 10 shows the 12 bands projected to be on the GOES-R series and the MODIS bands that have similar central wavelengths. Of the MODIS bands demonstrated here to be preferred for volcanic ash detection in the cases examined; that is, bands 28–32, only band 30 (9.7 μm) is not currently planned for the GOES-R series. This discrepancy should be considered if additional bands could be added to that instrument before it is built and launched.

6. Summary and conclusions

The 36 bands available on MODIS require sophisticated band-combination techniques such as PCIs to de-

TABLE 8. PCIs in descending order of qualitative value for ash cloud detection (Cleveland daytime case).

PCI No.	Qualitative assessment of ash contrast	Explained variance (%)	SNR
5	Ash extent	1.3	9.59
7	Ash extent, but lower contrast	0.52	2.57
4	Ash extent, but low contrast, and cloud contamination	4.0	6.57
14	Ash extent, but low contrast, and noisy	0.022	1.60
16	Ash/meteorological cloud distinction	0.003	1.95
8	Ash/meteorological cloud distinction (different)	0.36	2.59
6	Ash/densest meteorological cloud distinction, lower contrast	0.67	1.86
12	Ash/densest meteorological cloud distinction (different)	0.063	1.81

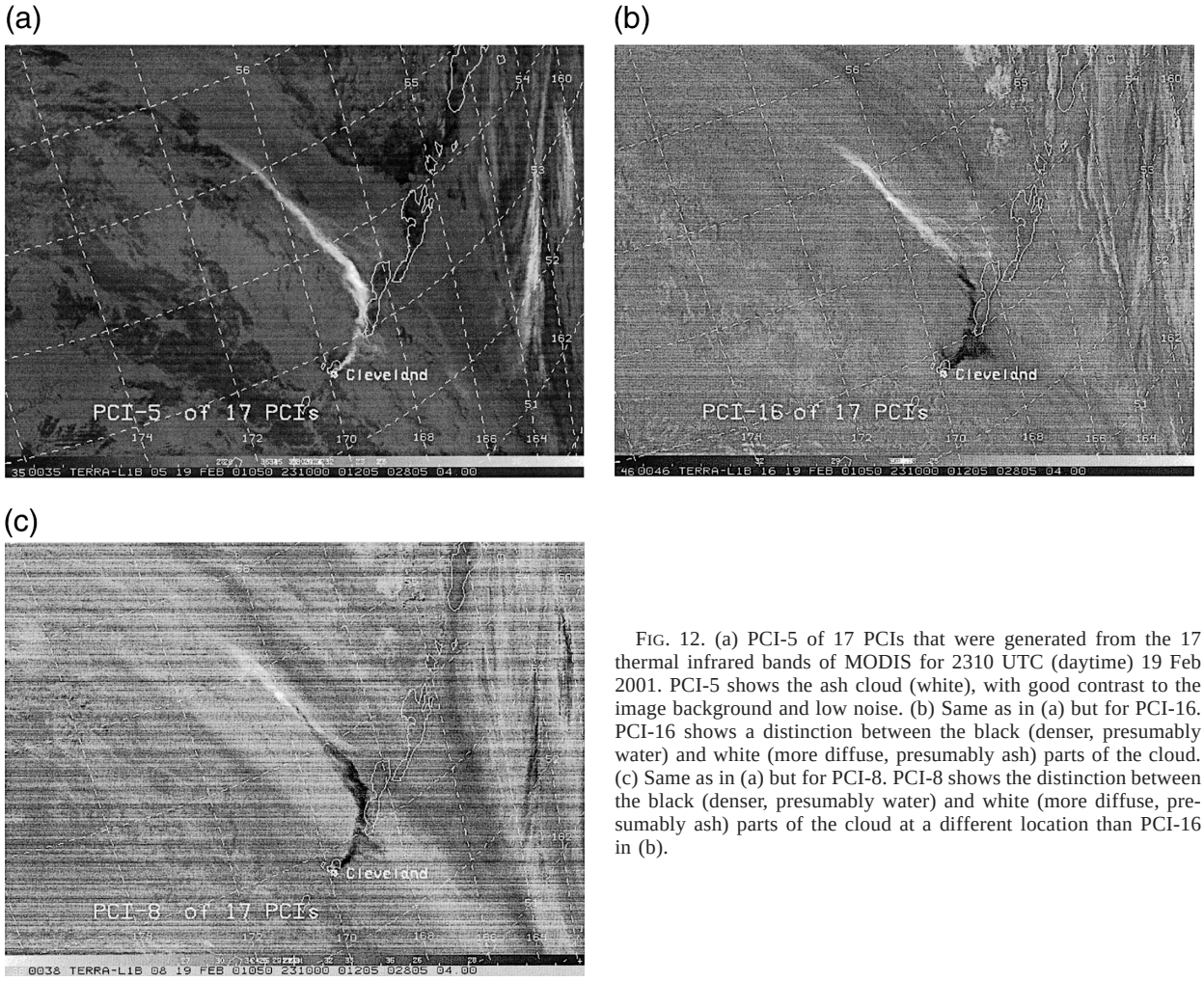

FIG. 12. (a) PCI-5 of 17 PCIs that were generated from the 17 thermal infrared bands of MODIS for 2310 UTC (daytime) 19 Feb 2001. PCI-5 shows the ash cloud (white), with good contrast to the image background and low noise. (b) Same as in (a) but for PCI-16. PCI-16 shows a distinction between the black (denser, presumably water) and white (more diffuse, presumably ash) parts of the cloud. (c) Same as in (a) but for PCI-8. PCI-8 shows the distinction between the black (denser, presumably water) and white (more diffuse, presumably ash) parts of the cloud at a different location than PCI-16 in (b).

termine the bands that are most suitable for detection of volcanic ash. Even though the explained variance of most of the PCIs is generally small, several of these image products provided sufficient signal above noise to locate the ash cloud with good contrast to the image background and other image features. While many of the MODIS bands contribute to ash detection, combinations of these bands in the form of various PCIs highlight variations in the ash cloud height and/or density and gas (e.g., SO_2) content, where the ash occurs at different levels, or has different particle concentrations. These applications of the PCI technique isolate MODIS band combinations that are the most useful and of significance for qualitatively detecting both the concentration and extent of the ash both day and night. However, since only two target volcanoes were examined, the specific results may not be directly applicable to other targets.

The multitude of MODIS bands gives much more flexibility for ash detection than the limited number of bands on the GOES Imager. The results of this study indicate that several of the MODIS bands are useful for volcanic ash detection. In particular, bands 28–32, in the water vapor and longwave portions of the spectrum, contributed most frequently to detection of the ash cloud. This includes bands 28–30 (7.3 to 9.7 μm) in the portion of the spectrum known for volcanic ash and gas signals. Bands 28 and 29 (7.3 and 8.6 μm, respectively), although not on the current GOES Imager, are planned for GOES-R. However, band 30 (9.7 μm) is neither available on the current GOES Imager nor planned for future GOES Imagers. Regardless, better ash cloud detection will be available with the increased number of bands and good temporal resolution available from the imagers planned for the GOES-R series.

Last, a word about PCI stability and potential weaknesses: Clouds can complicate and limit the ability to detect ash, just as they do for visible and infrared imagery. Significant differences can occur between day and night with the change in the reflected component of solar radiation. The composition of the PCIs is therefore case dependent. Different situations result in PCIs that are not identical combinations of the available band. For this reason PCIs are not necessarily the best tech-

TABLE 9. MODIS bands contributing heavily to the first six PCIs in Table 8 (in descending order of ash cloud contrast to the image background and other image features). Negative values are in parentheses. Boldface values are explained in text.

	Explained variance and sign of MODIS bands												
PCI	20 3.75 μm	23 4.05 μm	24 4.47 μm	25 4.52 μm	26 1.38 μm	27 6.7 μm	28 7.3 μm	29 8.6 μm	30 9.7 μm	31 11.0 μm	32 12.0 μm	33 13.3 μm	34 13.6 μm	35 13.9 μm	36 14.2 μm
5	(5.2%)	5.3%	0.7%	9.2%	**59.3%**	9.1%	(6.5%)	0.3%	0.1%	0.3%	1.5%	(~0%)	(0.5%)	(0.3%)	(1.0%)
7	(0.1%)	1.0%	1.1%	0.5%	(~0%)	~0%	2.6%	9.8%	**25.6%**	(0.3%)	(6.1%)	**(21.3%)**	13.3%	(0.5%)	17.1%
4	0.3%	(~0%)	4.4%	1.8%	3.5%	(9.5%)	(3.8%)	(10.6%)	4.8%	(5.6%)	(5.6%)	0.8%	18.1%	17.2%	13.7%
14	0.1%	(0.3%)	36.2%	(3.9%)	0.5%	(~0%)	(0.1%)	**23.6%**	**(20.9%)**	(0.7%)	(12.5%)	0.6%	~0%	0.5%	(~0%)
Sum of above	5.7%	6.6%	**42.4%**	15.4%	**63.3%**	18.6%	13.0%	**44.3%**	**51.4%**	6.9%	25.7%	22.7%	**31.9%**	18.5%	**31.8%**
16	~0%	(~0%)	~0%	1.2%	~0%	(~0%)	0.1%	(5.5%)	(0.1%)	**68.1%**	**(24.7%)**	(~0%)	(~0%)	(0.1%)	~0%
8	~0%	(0.1%)	(1.8%)	(1.1%)	18.4%	(14.1%)	**37.8%**	(0.4%)	(6.5%)	~0%	1.4%	3.8%	(2.4%)	(1.0%)	11.1%
Sum of all above	5.7%	6.7%	44.2%	17.7%	**81.7%**	32.7%	**50.9%**	**50.2%**	**58.0%**	**75.0%**	**51.8%**	26.5%	34.3%	19.6%	42.9%

TABLE 10. Comparison of 12-band GOES-R series Imager and MODIS bands.

GOES-R Imager		MODIS	
Band No.	Central wavelength (μm)	Band No.	Central wavelength (μm)
1	0.64	1	0.64
2	0.86	2	0.86
3	1.38	5	1.24
4	1.61	6	1.64
5	3.9	22	3.96
6	6.15	27	6.7
7	7.0	28	7.3
8	8.5	29	8.55
9	10.35	No equivalent	No equivalent
10	11.2	31	11.0
11	12.3	32	12.0
12	13.3	33	13.3

nique for direct operational applications, but can prove useful for determining combinations of the available band images for the detection of various atmospheric and surface features. The way to combine the bands may change, but there is benefit to be gained in knowing the bands that are of more value and those not of value. If the PCI technique shows that certain band combinations are preferable, those bands can be combined as specified by the PCIs to generate an operational product based on that training.

In Part II of this paper (Hillger and Clark 2002, this issue), MODIS data for the same volcanic cases examined above are used to simulate the impact of changes that will occur in spectral bands between current and near-term GOES imagery. The change from the 12.0-μm band to a 13.3-μm band on GOES-M (launched in 2001 and renamed *GOES-12*) was made to improve cloud-height determinations. However, when GOES-M becomes operational, the change in bands will have a potential negative impact on image products that are heavily utilized for volcanic ash detection. Image products generated from the three GOES infrared bands with the 13.3-μm band substituted for the 12.0-μm band, indicate that volcanic ash can be detected, but with diminished ability, especially for diffuse ash. For both day and night cases the increased contamination by clouds leads to increased chances of false ash detection for the cases examined. This potential loss in ash detectability is an additional motivation to develop new methods of ash detection to compensate for the loss of the 12.0-μm band from geostationary orbit for the next several years.

Acknowledgments. The MODIS data for this study were provided by Chris Moeller of the Cooperative Institute for Meteorological Satellite Studies (CIMSS) at the University of Wisconsin–Madison. Funding for this study is made available through NOAA Grant NA17RJ1228. Dr. Mark DeMaria and Dr. Bernie Connell provided helpful reviews of the manuscript.

APPENDIX

Basics of Principal Component Image Transformation

Principal components (PCs) have the ability to simplify multivariate data by reducing the dimensionality of the dataset (Gauch 1993). Features that are hidden in the data are brought out by PC analysis (Loughlin 1991). Principal component theory dictates that the information content of the PCs is compressed into the PCs in order of descending significance, with the lower-numbered PCs containing the primary information content, and the higher-numbered PCs containing other information and noise. Both Morrison (1976) and Preisendorfer (1988) give good graphical representations of the PC transformation process. The process can be summarized as a translation and rotation of the original coordinate system into a new coordinate system that better reflects the principal modes of variability in the dataset being analyzed.

Because of its ability to simplify multispectral datasets, PC (or eigenvector/eigenvalue analysis) analysis has been used extensively for the analysis of high-spatial-resolution environmental (land and ocean) remote-sensing imagery. However, the technique can also be used to analyze the information content of lower-spatial-resolution weather satellite imagery and has been termed principal component images (PCIs) by Hillger (1996a,b). Regardless of the intended application, the technique determines which part of the multispectral signal is common to all the images (spectral bands) and separates that information from other image information that is sensed only by image differences or multiple image combinations. Whereas the original images may (and often do) contain redundant information, the PCIs contain the independent signal separated out of the original images. This allows the image analyst to see the independent components of multispectral imagery.

Application to satellite imagery

The process of transforming multiband satellite imagery into PCIs is based on statistics generated from the images. Consider a set of imagery from N bands, viewing a scene at M horizontal locations (pixels, which includes data collected in scan lines and with a large number of samples in each line). At each pixel or location a vector of length N, denoted by $\mathbf{B}$, can represent the multiband imagery. A special linear transformation can be applied to provide a new vector of length N, denoted PCI as follows:

$$\mathrm{PCI} = \mathbf{E} \cdot \mathbf{B}, \tag{A1}$$

where $\mathbf{E}$ is an $N \times N$ matrix. For PCIs, the rows of $\mathbf{E}$ are the eigenvectors of the symmetric $N \times N$ covariance matrix with elements composed of covariances among the bands (summed over M pixel locations). The covariance matrix is generated from the imagery (or a subset of the imagery) being analyzed, and the eigenvectors are determined using a standard mathematical package for diagonalizing that matrix. The covariance matrix explains the relationships among the band images, allowing the eigenvector transform to parse that information into the PCIs. This parsing separates common and difference information from the multispectral imagery. The common information is concentrated into the PCIs in order of decreasing explained variance (the square of the eigenvalue), with PCI-1 containing most of the variance, and lesser variance in higher-numbered PCIs. The result of the eigenvector transformation is a restructuring of the satellite information into as many PCIs as there are available spectral-band images. (The PCIs can have no more degrees of freedom than the bands' images that are input.) The sum of the explained variances of the PCIs is equal to the sum of the explained variances of the original images—the same information content as the original imagery expressed in a new form.

The PCI concept is easier to explain when simplified to a small number of images or dimensions. In the simplest two-dimensional case, two band images, $\mathbf{b}_1$ and $\mathbf{b}_2$, are transformed into two PCIs, pci_1 and pci_2, using

$$\mathrm{pci}_1 = \mathbf{e}_1 \cdot \mathbf{b}_1 + \mathbf{e}_2 \cdot \mathbf{b}_2 \quad \text{and} \tag{A2}$$

$$\mathrm{pci}_2 = \mathbf{f}_1 \cdot \mathbf{b}_1 + \mathbf{f}_2 \cdot \mathbf{b}_2, \tag{A3}$$

where $\mathbf{e}$ and $\mathbf{f}$ are linear transformation vectors (eigenvectors, or rows in the eigenvector matrix $\mathbf{E}$) used to transform each pixel (or picture element) in the original band images into two PCIs. The individual **e**s and **f**s (eigenvector coefficients) can be positive or negative, for adding or subtracting the bands, as required by the transformation from bands into PCIs. With only two input bands, pci_1 contains the information that is common to the $\mathbf{b}_1$ and $\mathbf{b}_2$ images (an image sum), and pci_2 contains the information that is not shared, or that differs between the $\mathbf{b}_1$ and $\mathbf{b}_2$ images (an image difference). The three-band case can be visualized as a transformation of axes in three-dimensional space. For increasing numbers of images the transformation is increasingly harder to visualize.

REFERENCES

Dean, K., S. A. Bowling, G. Shaw, and H. Tanaka, 1994: Satellite analyses of movement and characteristics of the Redoubt volcano plume, January 8, 1990. *J. Volcanol. Geotherm. Res.*, **62,** 339–352.

Gauch, H. G., Jr., 1993: Prediction, parsimony, and noise. *Amer. Sci.*, **81,** 468–478.

Hillger, D. W., 1996a: Meteorological analysis using principal component image transformation of GOES imagery. *Proc. Int. Radiation Symp.–IRS'96: Current Problems in Atmospheric Radiation*, Fairbanks, AK, International Association of Meteorology and Atmospheric Physics, 480–483.

——, 1996b: Meteorological features from principal component image transformation of GOES imagery. *Proc. Int. Symp. on Optical Science, Engineering, and Instrumentation* (GOES-8 *and Beyond Conference*), Vol. 2812, Denver, CO, SPIE, 111–121.

——, and T. H. Vonder Haar, 1988: Estimating noise levels of remotely sensed measurements from satellites using spatial structure analysis. *J. Atmos. Oceanic Technol.,* **5,** 206–214.

——, and G. P. Ellrod, 2000: Detection of unusual atmospheric and surface features by employing principal component image transformation of GOES imagery, Preprints, *10th Conf. on Satellite Meteorology and Oceanography,* Long Beach, CA, Amer. Meteor. Soc., 461–464.

——, and J. D. Clark, 2002: Principal component image analysis of MODIS for volcanic ash. Part II: Simulation of current GOES and GOES-M imagers. *J. Appl. Meteor.,* **41,** 1003–1010.

Loughlin, W. P., 1991: Principal component analysis for alteration mapping. *Photogramm. Eng. Remote Sens.,* **57,** 1163–1169.

Morrison, D. F., 1976: *Multivariate Statistical Methods.* McGraw-Hill, 415 pp.

Oppenheimer, C., 1998: Volcanological applications of meteorological satellites. *Int. J. Remote Sens.,* **19,** 2829–2864.

Prata, A. J., 1989: Observations of volcanic ash clouds in the 10–12 μm window using AVHRR/2 data. *Int. J. Remote Sens.,* **10,** 751–761.

——, and I. F. Grant, 2001: Retrieval of microphysical and morphological properties of volcanic ash plumes from satellite data: Application to Mt. Ruapehu, New Zealand. *Quart. J. Roy. Meteor. Soc.,* **127,** 2153–2179.

——, G. Bluth, B. Rose, D. Schneider, and A. Tupper, 2001: Comments on ''Failures in detecting volcanic ash from a satellite-based technique.'' *Remote Sens. Environ.,* **78,** 341–346.

Preisendorfer, R. W., 1988: *Principal Component Analysis in Meteorology and Oceanography.* Elsevier, 425 pp.

Simpson, J. J., G. Hufford, D. Pieri, and J. Berg, 2000: Failures in detecting volcanic ash from a satellite-based technique. *Remote Sens. Environ.,* **72,** 191–217.

Washington VAAC, 1999: *Third Caribbean/South American Regional Air Navigation Meeting,* Buenos Aires, Argentina, International Civil Aviation Organization, 5 pp. [Available online at http://www.ssd.noaa.gov/VAAC/PAPERS/carsam.html.]